Rechargeable Mg-Ion Batteries Based on WSe_2 Nanowire Cathodes

Bin Liu,[†,‡] Tao Luo,[†] Guangyuan Mu,[†] Xianfu Wang,[†] Di Chen,[*,†] and Guozhen Shen[*,‡]

[†]Wuhan National Laboratory for Optoelectronics (WNLO) and College of Optical and Electronic Information, Huazhong University of Science and Technology (HUST), Wuhan 430074, P. R. China and [‡]State Key Laboratory for Superlattices and Microstructures, Institute of Semiconductors, Chinese Academy of Sciences, Beijing 100083, P. R. China

ABSTRACT The increasing interest in future energy storage technologies has generated the urgent need for alternative rechargeable magnesium ion batteries due to their innate merits in terms of raw abundance, theoretical capacity, and operational safety. Herein, we report an alternative pathway to a new energy storage regime: toward advanced rechargeable magnesium-ion batteries based on WSe_2 nanowire-assembled film cathodes. The as-grown electrodes delivered efficient Mg^{2+} intercalation/insertion activity, excellent cycling life, enhanced specific capacity, and excellent rate capability. We also evaluated the influence of Mg-intercalation behavior on Mg-ion batteries based on WSe_2 film cathodes *via* the first-principles DFT computations. The results reveal the feasibility of using advanced magnesium-ion batteries based on WSe_2 film as energy storage components in next-generation optoelectronic systems.

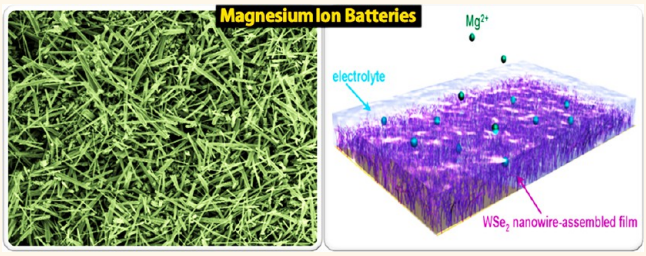

KEYWORDS: magnesium-ion batteries · WSe_2 nanowire-assembled film · alternative energy-storage option · superior performance · promising applications

Currently, rechargeable lithium ion batteries have been widely applied in portable consumer electronics and are further expected to power electric vehicles and even to be used in stationary electric-grid harvesting from renewable energy sources.[1−15] Although successful commercialization of Li ion batteries has greatly promoted technological advancements, it is well-known that the currently available lithium batteries have several drawbacks including limited/unevenly distributed lithium resource, low power density, worries about safety, short service life, and high production cost, which greatly impact their use for next-generation large-scale commercial manufacture of energy storage units.[16] Compared to lithium batteries, magnesium batteries have been considered as a future prospective candidate for reversible energy storage and conversion owing to the greater abundance of magnesium resources (1.94%) than lithium (0.006%), more stability of metallic Mg in humid and oxygen environment, higher expected safety and lower relative toxicity, and high specific capacity (2205 Ah kg^{-1}).[17−22] Furthermore, it is of importance primarily that Mg and Li elements have greatly similar chemical properties due to their unique diagonal rule of the Periodic Table of Elements. Therefore, worldwide studies on rechargeable advanced magnesium ion batteries could lead to an alternative pathway to a new energy storage regime.

So far, only a few Mg^{2+} insertion cathodes can illustrate reasonable reversible capacity and short cycle number in the rechargeable Mg battery systems, including MoS_2,[17,20,23] $CuyMo_6S_8$,[24] $Mg_{1.03}Mn_{0.97}SiO_4$,[25] and TiS_2.[26] The major issues for magnesium ion batteries are kinetically torpid reversible Mg^{2+} insertion/extraction and diffusion in Mg-insertion cathodes due to the strong polarization effect of the divalent Mg^{2+} compared with Li^+.[17,19,20] Among other potential electrodes, WSe_2, a layer-structured metal chalcogenide, has gained increasing attention recently owing to its extraordinary characteristics of ultralow thermal conductivity,[27] highly hydrophobic sticky surfaces,[28] and efficient p-type field-effect properties.[29] To date, little attention has been paid to their energy storage features. In addition, although several synthetic routes for WSe_2 samples were mentioned, no report has been found on the synthesis of unique 1D WSe_2 nanowires by

* Address correspondence to gzshen@semi.ac.cn, dichen@mail.hust.edu.cn.

Received for review June 26, 2013 and accepted August 8, 2013.

Published online August 08, 2013
10.1021/nn4032454

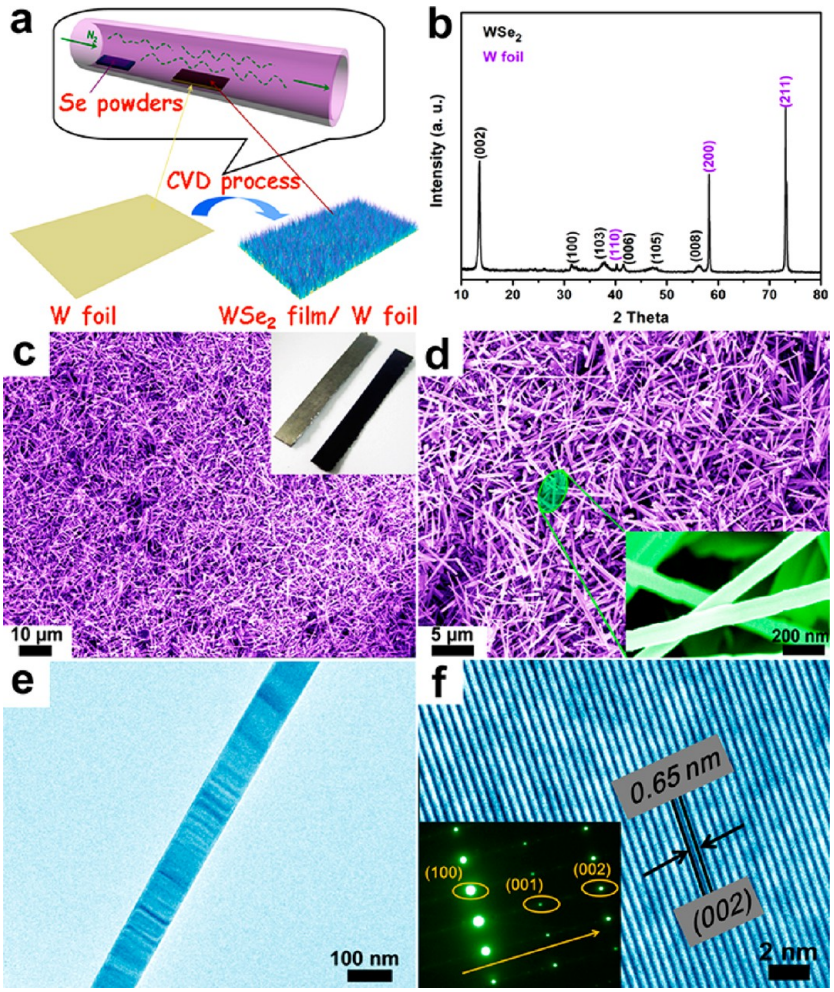

Figure 1. Sample fabrication and morphology characterization. (a) Schematic illustration of the CVD procedures for the growth of WSe_2 nanowire film on W foil and its corresponding (b) XRD pattern, (c, d) SEM, and (e, f) TEM images. Inset is the SAED pattern.

utilizing W foil as both tungsten resource and substrate. It is expected that advancements in future storage technology could be gained by incorporating novel WSe_2 nanostructured cathodes into advanced rechargeable magnesium ion batteries.

Herein, we report on the discovery of WSe_2 nanowire-assembled film/W foil composites as cathodes for next-generation rechargeable magnesium ion batteries. The as-fabricated rechargeable Mg ion batteries composed of WSe_2 cathodes and Mg anodes delivered efficient Mg^{2+} intercalation/insertion activity, outstanding cycling life, enhanced specific capacity, and excellent rate capability. Further, we calculated and simulated the crucial parameters for comparison between WSe_2 and $Mg_{0.67}WSe_2$ in electrochemical processes *via* first-principles DFT computations, such as the electron density, band structure, mobility, and density of state, evaluating the major merits of these Mg^{2+} insertion-based WSe_2 electrodes corresponding to related experiment data. Our findings have provided a technical feasibility of considerable Mg^{2+} intercalation and deintercalation inside the as-synthesized unlimited-potential cathodes, which opens up new opportunities for rechargeable Mg batteries.

RESULTS AND DISCUSSION

WSe_2 nanowire-assembled film was synthesized *via* a chemical vapor deposition (CVD) route from the reaction of Se powder and W foil. Figure 1a shows the drawing of the fabrication process of WSe_2 film grown on the W foil. From the plot, we can see that Se powders placed at the entrance of quartz tube were separated from W foil at the center of one. When applied a certain temperature, Se powders were evaporated, carried by the N_2 gas, and reacted with the tungsten substrate at 900 °C to form into WSe_2 nanowire film. More details of the synthesis are described in the Experimental Section. The corresponding XRD pattern of the as-obtained samples is illustrated in Figure 1b. All peaks are indexed to the hexagonal WSe_2 (JCPDS No. 38-1388) except three peaks from W foil, which indicated the high purity of the as-fabricated WSe_2 nanowire-assembled film. Figure 1c inset clearly shows the change of the substrate color,

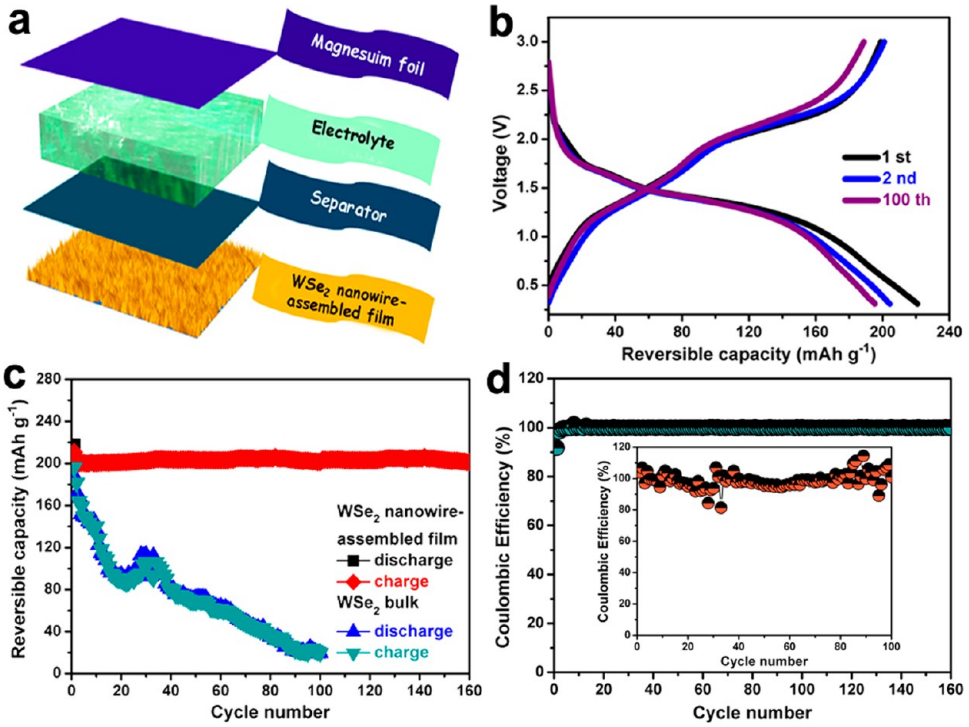

Figure 2. Electrochemical properties of the coin-type batteries measured at a current density of 50 mA g^{-1} between 0.3 and 3 V: (a) schematic representation of the as-assembled cell composed of magnesium foil anode, electrolyte, separator, WSe_2 film cathode, (b) charge/discharge curves, (c) cycling performance, and (d) coulombic efficiency (CE).

indicating the deposition of WSe_2 samples on the W foil. The morphology of the as-deposited samples was characterized by scanning electron microscopy (SEM) and transmission electron microscopy (TEM) techniques. Parts c and d of Figure 1 illustrate the SEM images of the as-prepared film on the surface of W foil, showing the deposition of numerous nanowires on the whole foil. Typical nanowires have diameters of ~100 nm and ~7 , as can be seen in the Figure 1d inset. Figures 1e−f shows the corresponding TEM and high-resolution TEM (HRTEM) images of a single nanowire with a diameter of about 100 nm. The clearly resolved lattice fringe is measured to be about 0.65 nm, corresponding well to the (002) plane of WSe_2. Combined with the relevant selected-area electron diffraction (SAED) pattern inset, it is concluded that single crystalline WSe_2 nanowires are successfully synthesized *via* the current CVD process.

To measure the electrochemical properties of the as-grown WSe_2 nanowire-based electrode, we fabricated coin-shaped cells by assembling magnesium foil (anode), electrolyte, separator, and WSe_2 nanowire-based electrode (cathode) into a complete magnesium-ion battery unit and the corresponding diagram was depicted in Figure 2a. The electrolyte used for the Mg battery was prepared *via* a chemical route according to previous report, and Figure S1 (Supporting Information) displays the reaction equation of electrolyte.[30] Briefly, $Mg(AlCl_2EtBu)_2$ was first prepared by mixing proper amounts of Bu_2Mg solution (1 M in hexane, Aldrich) and $AlCl_2Et$ solution (1 M in heptane, Aldrich) in a 1:2 stoichiometric ratio. Then the prepared $Mg(AlCl_2EtBu)_2$ was dissolved in THF solution to form the 0.25 mol g^{-1} $Mg(AlCl_2EtBu)_2$/THF electrolyte.

Figure 2b shows the voltage profiles of the WSe_2-based electrodes between 0.3 and 3 V at a current density of 50 mA g^{-1} for 160 cycles, revealing the discharge platform is approximately 1.6 V and the decay of specific capacity is very little. Accordingly, Figure 2c displays the cycling performance of these electrodes over 160 cycles. From the plot, we can clearly see that the reversible specific capacity of these electrodes keeps at a quite considerable value around 203 mAh g^{-1} for all of the cycles, showing their high specific capacitance and excellent cycling stability for Mg ion battery application, while the as-prepared WSe_2 bulk electrodes that was also evaluated by using the same conditions as the above WSe_2 nanowires cathodes displayed significantly inferior cycling performance with even a low capacity retention of 10% after 100 cycles (typical SEM images of WSe_2 bulk, as shown in Figure S2). It reveals that our unique one-dimensional-assembled WSe_2 architectures with high stability and numerous active sites/channels may greatly contribute to their electrochemical properties. According to previous report, a unit of $Mg_{0.67}WSe_2$ ($Mg_4W_6Se_{12}$) as stable phase is obtained, which consistent with results of the other Mg-insertion chalcogenide-cathode ($Mg_4Mo_6S_{12}$).[20] Also, it may be concluded that the total electrochemical processes of our prepared WSe_2-based cathodes during

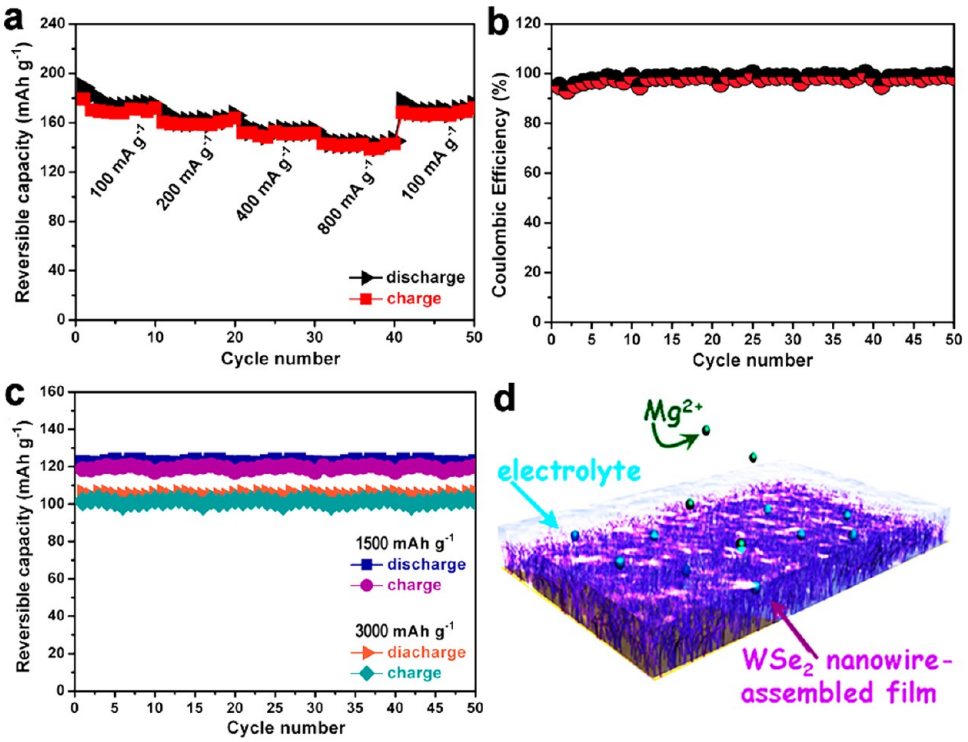

Figure 3. Rate-capability analysis of these electrodes. (a) Rate performance of the WSe_2-based electrodes at various current densities. (b) The corresponding CE. (c) Long cycling performance of these electrodes at large rates of 1500 and 3000 mA g-1. (d) Schematic of operation principle of rechargeable magnesium-ion batteries based on WSe_2 nanowire-assembled film.

the charge/discharge cycles are expressed as follows:

$$6WSe_2 + 4Mg^{2+} + 8e^- \leftrightarrow Mg_4W_6Se_{12} \text{ (cathode)}$$

$$4Mg \leftrightarrow 4Mg^{2+} + 8e^- \text{ (anode)}$$

$$6WSe_2 + 4Mg \leftrightarrow Mg_4W_6Se_{12} \text{ (total)}$$

The corresponding coulombic efficiency (CE) of the WSe_2 nanowire-assembled film and WSe_2 bulk electrodes are shown in Figure 2d and its inset, which is around 98.5% for as long as 160 cycles and 93.8% for 50 cycles, respectively, indicating that the WSe_2 nanowire-assembled film electrodes delivered very more efficient and stable electrochemical behaviors compared to bulk samples. It reveals that these WSe_2 nanowire-based electrodes fit well for various high-performance new storage systems.

To evaluate the rate performance of the WSe_2 nanowire-based electrode, we measured the rate capacity at different current density ranging from 100, 200, 400 to 800 mA g^{-1} for 50 cycles between 0.3 and 3 V, respectively. From Figure 3a, we can see that even at a high current density of 800 mA g^{-1}, the specific capacity is still kept at 142 mAh g^{-1} (a retention of as high as 83.5%). Besides, a capacity of 168 mAh g^{-1} at 100 mA g^{-1} is retained after 40 discharge/charge cycles at various preceding current densities (100, 200, 400, and 800 mA g^{-1}), indicating the very good structural stability of the WSe_2 nanowire-based electrodes. The corresponding CE also reached a high level (~98.8%), indicating an efficient electrochemical activities of the current cathodes (Figure 3b).

Higher charging current densities of 1500 and 3000 mA g^{-1} were also applied to further evaluate the rate capability of the as-fabricated electrodes, and the results are demonstrated in Figure 3c. The electrodes were found to deliver capacity of 120 mAh g^{-1} at 1500 mA g^{-1} and 103 mAh g^{-1} at 3000 mA g^{-1} for 50 charge/discharge cycles, illustrating their superior cycling performance and excellent rate capability. Until now, in terms of stability, cycling, and rate capability as critical measurable parameters, our results for these WSe_2 nanowire-assembled film cathodes are clearly superior to the electrochemical features of other reported Mg-insertion materials, as shown in Table S1 (Supporting Information). Inspiring comprehensive performance of these novel WSe_2 electrodes for rechargeable Mg-ion batteries may greatly contribute to further development of desired energy storage components, which may facilitate new growth points of battery industry. Figure 3d vividly represents the operation merits of the current WSe_2 nanowire film cathodes during electrochemical processes. Briefly, the advancements in the current WSe_2 nanowire film cathodes based magnesium-ion battery units might be due to the following reasons: In Figure 3d, we can find that the 3D-composite network architecture composed of WSe_2 nanowire-assembled film (purple layer) and W foil (yellow plane) could greatly enhance effective contact area between the electrolyte (wathet blue area) and numerous nanowires, facilitating magnesium-ion (green small sphere)/electron transport inside active

materials and diffusion of the electrolyte to show the greatly efficient performance for Mg cells. This WSe_2 nanowire-assembled architecture/W foil matrix can achieve an excellent electronic conductivity due to the WSe_2 nanowires directly grown on the W substrate to form very electrical contact and good adhesion, building up an expressway for charge transfer in total storage system. The unique WSe_2 nanowires with one-dimensionality are beneficial to the free insertion/extraction of Mg^{2+} among layered WSe_2, which also shorten the charge transfer pathway and lower the exchange resistance for the magnesium ions between active functional materials and electrolyte.[31−33] In addition, the anodic stability of $Mg(AlCl_2BuEt)_2$ is clearly superior to that of the other electrolytes.[17] This electrolyte does not develop strongly passivating films on the Mg surface, and the deposition/dissolution of Mg is almost 100% reversible.[34] As-prepared $Mg(AlCl_2BuEt)_2$/THF has been regarded as a greatly suitable and efficient electrolyte because it may partially reduce the polarization effect, make maximized Mg-ion insertion behavior, and guarantee reasonable cycling performance of Mg-ion batteries. Finally, according to the above XRD pattern and HRTEM image, it can be revealed that the high-crystallinity and purity resulting samples are achieved by high temperature CVD process, which contributes to their corresponding excellent performance. Thus, considering these above results, only in this novel storage unit can we obtain desirous advanced features of the magnesium ion batteries.

Toward new-type promising batteries, such as Li−S, Mg ion, and Na ion batteries, their indispensable cycling stability has been paid less attention compared with the existing Li ion batteries. Fortunately, our results here clearly demonstrate the excellent cycling stability of the current WSe_2 nanowire-based electrodes. To give more directly evidence, we also measured the SEM images of the electrode before and after cycled for 80 charge/discharge cycles at 100 mA g^{-1}. As can be seen in Figure 4 and Figure S3 (Supporting Information), the WSe_2 nanowires did not show obvious morphology change, confirming their attractive morphological stability during electrochemical reactions. It is worth mentioning that all of the above effects will undoubtedly make it possible to achieve high-performance future Mg-ion batteries based on the current grapheme-like WSe_2 nanowire-assembled film cathodes.

In order to appropriately evaluate the obtained results of the current WSe_2 nanowire-based electrodes, the first-principles density functional theory (DFT) was further applied to analyze the features of the electrode. Figure 5a shows the structural model of the layer-structured WSe_2 intercalated with Mg, where the Mg was found intercalated on two WSe_2 layers. A formula unit of $W_{16}Se_{32}$ is thus chosen as a representative of a WSe_2 monolayer for the investigation of Mg intercalation and each Mg atom is coordinated by three Se atoms at a distance of 2.5 Å. Figure 5b shows the side

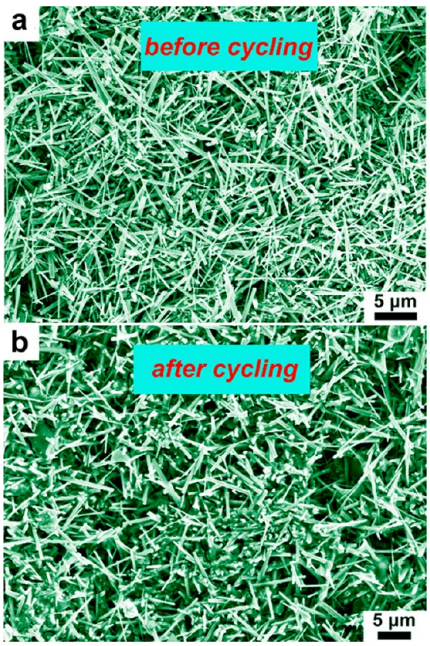

Figure 4. Structure stability of the WSe_2-electrode cycled at 50 mA g^{-1} over 80 cycles. SEM images of the samples (a) before and (b) after 80 cycling.

view image of the Mg intercalated WSe_2 structure, where every two neighboring layers can form a cycling period in layered WSe_2 structures. The top view image in Figure 5c shows that a single WSe_2 layer is fully intercalated by Mg atoms on both sides and a maximum of four Mg atoms could be inserted on each side of the layer. A formula unit of $Mg_4W_6Se_{12}$ ($Mg_{0.67}WSe_2$) is thus selected as a simulation object (marked with a blue rectangle in Figure 5c), corresponding to the above experimental electrochemical results of the WSe_2 cathodes.

Based on the above models, many vital parameters, such as the electron density, the band structure, the mobility, and DOS, were calculated progressively according to the first-principles DFT. In parts d and e of Figure 5, the dotted green boxes of both WSe_2 and $Mg_{0.67}WSe_2$ are constructed to form the brillouin zone related to their band structure. The corresponding purple dotted isosurfaces exhibit the electron density features of two compounds. From Figure 5e we can see that the isosurfaces among neighboring $Mg_{0.67}WSe_2$ layers not only still keep the respective smooth matrix but also do not stagger or overlap each other when Mg ions were fully intercalated, showing outstanding feasibility and stability of such a structure in the cathode materials and likely facilitating the electrochemical stability in the charge/discharge experiments for these WSe_2 electrodes.

The band structures of WSe_2 and $Mg_{0.67}WSe_2$ are illustrated in parts f and g, respectively, of Figure 5. In Figure 5f, the simulated direct band gap of WSe_2 is 1.33 eV, in good agreement with the reported data, confirming the reliability of our simulation. Besides, the conduction band minimum (CBM) is located in 1.33 eV and the valence band maximum (VBM) is located in 0 eV,

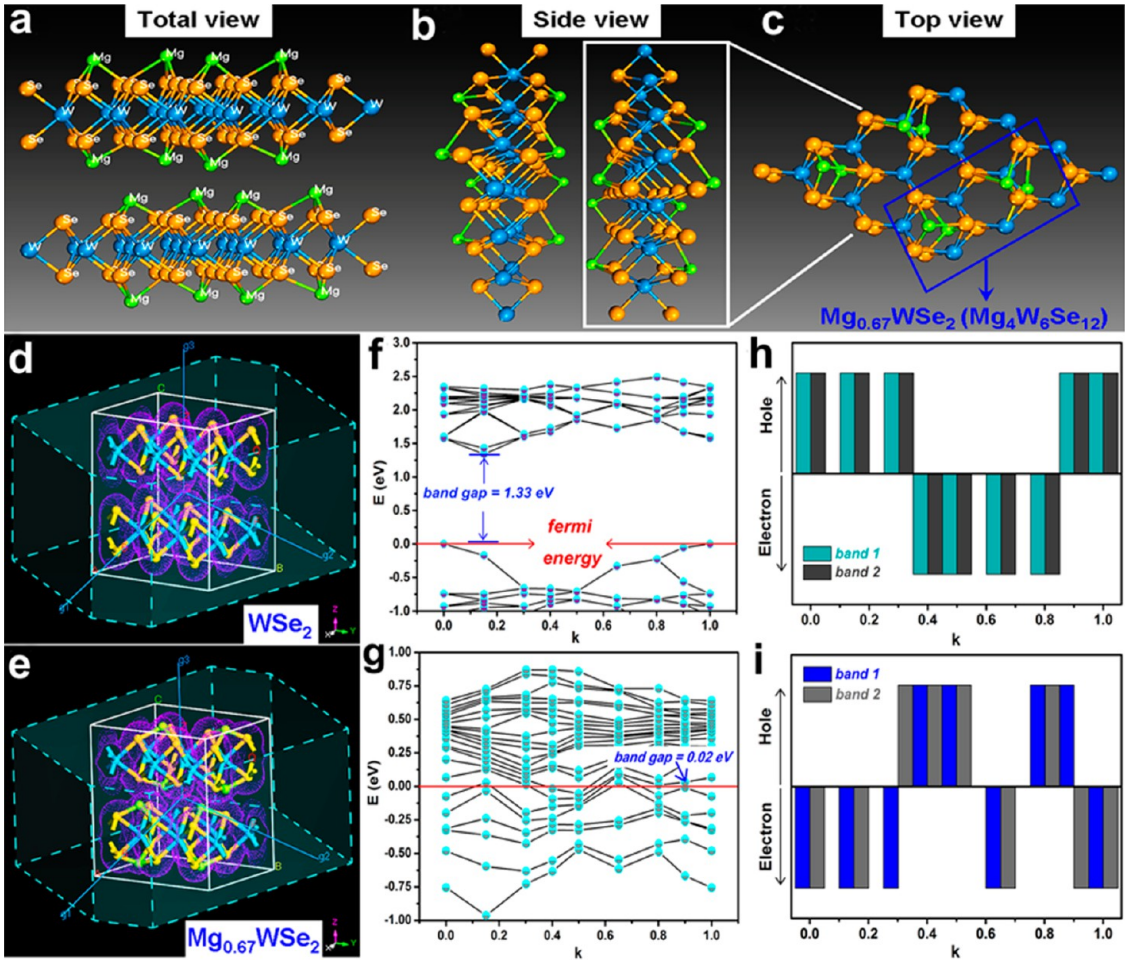

Figure 5. Structure model and computational simulation. (a–c) Graphical illustrations of theoretically modeled Mg intercalation on the graphene-like WSe_2 single layer (green spheres. Mg atoms; orange spheres, Se atoms; blue spheres, W atoms). Comparison of (d, e) the electron density, (f, g) the band structure, and (h, i) the proportion of electrons and holes for WSe_2 and $Mg_{0.67}WSe_2$.

which defaults to the Fermi level. Once intercalated with Mg ions, $Mg_{0.67}WSe_2$ was obtained and the band gap of the formed $Mg_{0.67}WSe_2$ reduces to 0.02 eV, as shown in Figure 5g, indicating the electrical conductivity of WSe_2 changing from semiconductor to almost conductor. To further study the electrical properties of the samples, comparison of the mobility between the two compounds is given in Figure 5h,i. The corresponding 18 data points from two bands in the bottom of the conduction bands of the two compounds are demonstrated in parts f and g, respectively, of Figure 5. Compared to the electron ratio of WSe_2, the proportion of electrons can be remarkably increased when Mg ion is fully intercalated into WSe_2 to form $Mg_{0.67}WSe_2$. As is known, the mobility of electrons is higher than that of holes in the same condition. To get more information about the Mg-intercalation influence on WSe_2, the density of state (DOS) of Mg, WSe_2, and $Mg_{0.67}WSe_2$ were also calculated (Figures S4–6, Supporting Information). The weak peak from the DOS curve of Mg cross the Fermi level (0 eV), as shown in Figure S4 (Supporting Information), indicates its relevant metallic feature. Figure S5 (Supporting Information) shows the DOS curves of WSe_2, revealing their obvious semiconductor properties due to the strong peak in −38 eV and most of the electrons are converged in valence bands. While compared with the DOS curves of WSe_2, we find that the several peaks near Fermi level of $Mg_{0.67}WSe_2$ moved left, which indicates more electrons are transferred in the lower energy filed and the electron states of being activated are weaker (Figure S6).[35] It indicates that the electrochemical properties of $Mg_{0.67}WSe_2$ cathodes tend to be stable, which is beneficial to enhance the performance of $Mg_{0.67}WSe_2$ samples for promising magnesium ion batteries. All of the above theoretical and simulation results, together with the experimental results, reveal that the current WSe_2 samples as a new class of high-performance electrodes are suitable candidates for future alternative Mg ion storage units.

CONCLUSIONS

In summary, we presented the synthesis of the WSe_2 nanowire-assembled film as binder-free cathodes for

promising magnesium ion batteries. It is worth mentioning that all obtained results, including both experimental data and theoretical simulations, revealed that the as-prepared WSe_2-based electrodes delivered the unique electrochemical performances, such as efficient Mg^{2+} intercalation/insertion activity, stable specific capacity, outstanding cycling life, and excellent rate capability. Our work opens up a new alternative energy storage option for powering zero emission EV vehicles, portable electric devices, and photovoltaic devices.

EXPERIMENTAL METHODS

Preparation of the $Mg(AlCl_2EtBu)_2$/THF Electrolyte. A white solid precipitation formed immediately when the proper amounts of $MgBu_2$ solution (1 M in hexane, Aldrich) and $AlEtCl_2$ solution (1 M in heptane, Aldrich) in a ratio of 1:2 were mixed at room temperature. After stirred for 24 h, the hexane and heptane solutions were completely evaporated and a proper amount of high-purity tetrahydrofuran (THF) was slowly added to form the desired 0.25 mol L^{-1} solution as Mg-battery electrolyte. The above reactions were performed in an argon-filled glovebox (MBraun, Germany) with oxygen and water concentrations less than 1 ppm.

Synthesis of WSe_2 Nanowire-Assembled Film. In a typical procedure, a polished tungsten foil located at a ceramic boat was placed in the center of a tube furnace (Lindberg, USA), and then another ceramic boat holding selenium powder (0.1 g, Aldrich) was placed in the upwind low-temperature zone of the tube furnace. The furnace was first purged with high-purity N_2 with a flow rate of 500 sccm for 20 min and then heated to 800 °C at a rate of 10 °C/min with a N_2 flow rate of 50 sccm and kept at that temperature for 2 h. The as-obtained samples were characterized with X-ray diffractometer (XRD; X' Pert PRO, PANalytical B.V.) with radiation from a Cu target (K_α, $\lambda = 0.15406$ nm). The morphologies of the samples were observed by field emission scanning electron microscopy (FE-SEM; Sirion 200) and transmission electron microscopy (TEM; Philips CM 20).

Cell Assembly and Electrochemical Characterization. Electrochemical experiments were performed using CR2032-type coin cells with Celgard 2400 membrane as separator and polished magnesium-foil as anode electrode in the voltage range of 0.3−3 V versus Mg/Mg^{2+} at the room temperature. The electrolyte was as-synthesized 0.25 mol L^{-1} $Mg(AlCl_2EtBu)_2$/THF. The cathode electrode was binder-free WSe_2 nanowire-assembled film directly coated on W foil from the CVD growth. The loading density of active material on tungsten substrate here was 3−4 mg cm^{-2}. The cells were assembled in an argon-filled glovebox with oxygen and water contents less than 1 ppm. The electrochemical performances were evaluated on a LAND battery test system (Wuhan, China) at the room temperature.

Computational Methods. Density functional theory (DFT) is a quantum mechanical modeling method used in physics and chemistry to investigate the electronic structure of many-body systems, in particular, molecules. Thus, for our models of WSe_2 and $Mg_{0.67}WSe_2$, the first-principles DFT computations were performed using a plane wave basis set with the projector-augmented plane wave (PAW)[36] to model the ion-electron interaction in the Cambridge Sequential Total Energy Package (CASTEP). The generalized gradient approximation with the PBE[37] functional and a 310 eV cutoff for the plane wave basis set and the convergence in energy and force (10^{-6} eV and 10^{-2} eV $Å^{-1}$) were adopted in all of the computations, respectively. The following electronic states were treated as valence: Mg, $2p^63s^2$ (converged in 20 iterations to a total energy of −972.1662 eV), Se, $4s^24p^4$ (converged in 17 iterations to a total energy of −256.4674 eV), and W, $5s^25p^65d^46s^2$ (converged in 26 iterations to a total energy of −1922.2989 eV). Also, 2*1*1 k points, $2.0e^{-6}$ eV/atom SCF tolerance, and max SCF cycles (100) were then used to calculate the electronic band structure. Electronic parameters are listed as follows: number of electrons (376), number of up spins (188), number of down spins (188), and number of bands (188).

Conflict of Interest: The authors declare no competing financial interest.

Supporting Information Available: Preparation of electrolyte for Mg-ion batteries, morphology characterization of WSe_2 bulk, SEM images of WSe_2 nanowire-assembled film after cycling, density of state (DOS) characterization, and comparison of the desired performance between existing WSe_2 cathodes and other reported Mg-insertion electrodes. This information is available free of charge *via* the Internet at http://pubs.acs.org.

Acknowledgment. This work was supported by the National Natural Science Foundation (51002059, 21001046), the 973 Program of China (2011CB933300), and the Program for New Century Excellent Talents of the University in China (Grant No. NCET-11-0179). Special thanks to the Analytical and Testing Center of HUST and the Center of Micro-Fabrication and Characterization (CMFC) of WNLO for using their facilities.

REFERENCES AND NOTES

1. Kovalenko, I.; Zdyrko, B.; Magasinski, A.; Hertzberg, B.; Milicev, Z.; Burtovyy, R.; Luzinov, I.; Yushin, G. A Major Constituent of Brown Algae for Use in High-Capacity Li-Ion Batteries. *Science* **2011**, *334*, 75–79.
2. Jung, H. G.; Jang, M. W.; Hassoun, J.; Sun, Y. K.; Scrosati, B. A High-Rate Long-Life $Li_4Ti_5O_{12}$/$Li[Ni_{0.45}Co_{0.1}Mn_{1.45}]O_4$ Lithium-Ion Battery. *Nature Commun.* **2011**, *2*, 516–520.
3. Xu, Y. H.; Zhu, Y. J.; Liu, Y. H.; Wang, C. S. Electrochemical Performance of Porous Carbon/Tin Composite Anodes for Sodium-Ion and Lithium-Ion Batteries. *Adv. Energy Mater.* **2013**, *3*, 128–133.
4. Hu, L. B; Kim, H. S.; Lee, J. Y.; Peumans, P.; Cui, Y. Scalable Coating and Properties of Transparent, Flexible, Silver Nanowire Electrodes. *ACS Nano* **2010**, *4*, 2955–2963.
5. Park, M. H.; Kim, M. G.; Joo, J.; Kim, K.; Kim, J.; Ahn, S.; Cui, Y.; Cho, J. Silicon Nanotube Battery Anodes. *Nano Lett.* **2009**, *9*, 3844–3847.
6. Ge, M. Y.; Rong, J. P.; Fang, X.; Zhou, C. W. Porous Doped Silicon Nanowires for Lithium Ion Battery Anode with Long Cycle Life. *Nano Lett.* **2012**, *12*, 2318–2323.
7. Liu, B.; Zhang, J.; Wang, X. F.; Chen, G.; Chen, D.; Zhou, C. W.; Shen, G. Z. Hierarchical Three-Dimensional $ZnCo_2O_4$ Nanowire Arrays/Carbon Cloth Anodes for A Novel Class of High-Performance Flexible Lithium-Ion Batteries. *Nano Lett.* **2012**, *12*, 3005–3011.
8. Ellis, B. L.; Makahnouk, W. R. M.; Makimura, Y.; Toghill, K.; Nazar, L. F. A Multifunctional 3.5 V Iron-Based Phosphate Cathode for Rechargeable Batteries. *Nat. Mater.* **2007**, *6*, 749–753.
9. Wang, G. M.; Lu, X. H.; Ling, Y. C.; Zhai, T.; Wang, H. Y.; Tong, Y. X.; Li, Y. LiCl/PVA Gel Electrolyte Stabilizes Vanadium Oxide Nanowire Electrodes for Pseudocapacitors. *ACS Nano* **2012**, *6*, 10296–10302.
10. Wang, H. L.; Yang, Y.; Liang, Y. Y.; Zheng, G. Y.; Li, Y. G.; Cui, Y.; Dai, H. J. Rechargeable Li-O_2 Batteries with A Covalently Coupled $MnCo_2O_4$-Graphene Hybrid as An Oxygen Cathode Catalyst. *Energy Environ. Sci.* **2012**, *5*, 7931–7935.
11. Luo, S.; Wang, K.; Wang, J. P.; Jiang, K. L.; Li, Q. Q.; Fan, S. S. Binder-Free $LiCoO_2$/Carbon Nanotube Cathodes for High-Performance Lithium Ion Batteries. *Adv. Mater.* **2012**, *24*, 2294–2298.
12. Zhang, G. Q.; Yu, L.; Wu, H. B.; Hoster, H. E.; Lou, X. W. Formation of Ball-in-Ball Hollow $ZnMn_2O_4$ Microspheres as A High-Performance Anode for Lithium-Ion Batteries. *Adv. Mater.* **2012**, *24*, 4609–4613.
13. Cao, F. F.; Deng, J. W.; Xin, S.; Ji, H. X.; Schmidt, O. G.; Wan, L. J.; Guo, Y. G. Cu-Si Nanocable Arrays as High-Rate Anode Materials for Lithium-Ion Batteries. *Adv. Mater.* **2011**, *23*, 4415–4420.

14. Gowda, S. R.; Pushparaj, V.; Herle, S.; Girishkumar, G.; Gordon, J. G.; Gullapalli, H.; Zhan, X. B.; Ajayan, P. M.; Reddy, A. L. M. Three-Dimensionally Engineered Porous Silicon Electrodes for Li Ion Batteries. *Nano Lett.* **2012**, *12*, 6060–6065.
15. Park, M. H.; Cho, Y.; Kim, K.; Kim, J.; Liu, M. L.; Cho, J. Germanium Nanotubes Prepared by Using the Kirkendall Effect as Anodes for High-Rate Lithium Batteries. *Angew. Chem., Int. Ed.* **2011**, *50*, 9647–9650.
16. Peng, B.; Liang, J.; Tao, Z. L.; Chen, J. Magnesium Nanostructures for Energy Storage and Conversion. *J. Mater. Chem.* **2009**, *19*, 2877–2883.
17. Aurbach, D.; Lu, Z.; Schechter, A.; Gofer, Y.; Gizbar, H.; Turgeman, R.; Cohen, Y.; Moshkovich, M.; Levi, E. Prototype Systems for Rechargeable Magnesium Batteries. *Nature* **2000**, *407*, 724–727.
18. Guo, Y. S.; Zhang, F.; Yang, J.; Wang, F. F.; NuLi, Y. N.; Hirano, S. Boron-Based Electrolyte Solutions with Wide Electrochemical Windows for Rechargeable Magnesium Batteries. *Energy Environ. Sci.* **2012**, *5*, 9100–9106.
19. NuLi, Y. N.; Yang, J.; Wang, J. L.; Li, Y. Electrochemical Intercalation of Mg^{2+} in Magnesium Manganese Silicate and Its Application as High-Energy Rechargeable Magnesium Battery Cathode. *J. Phys. Chem. C* **2009**, *113*, 12594–12597.
20. Liang, Y. L.; Feng, R. J.; Yang, S. Q.; Ma, H.; Liang, J.; Chen, J. Rechargeable Mg Batteries with Graphene-Like MoS_2 Cathode and Ultrasmall Mg Nanoparticle Anode. *Adv. Mater.* **2011**, *23*, 640–643.
21. Li, C. S.; Cheng, F. Y.; Ji, W. Q.; Tao, Z. L.; Chen, J. Magnesium Microspheres and Nanospheres: Morphology-Controlled Synthesis and Application in Mg/MnO_2 Batteries. *Nano Res.* **2009**, *2*, 713–721.
22. Novak, P.; Imhof, R.; Haas, O. Magnesium Insertion Electrodes for Rechargeable Nonaqueous Batteries—A Competitive Alternative to Lithium? *Electrochim. Acta* **1999**, *45*, 351–367.
23. Aurbach, D.; Suresh, G. S.; Levi, E.; Mitelman, A.; Mizrahi, O.; Chusid, O.; Brunelli, M. Progress in Rechargeable Magnesium Battery Technology. *Adv. Mater.* **2007**, *19*, 4260–4267.
24. Mitelman, A.; Levi, M. D.; Lancry, E.; Levi, E.; Aurbach, D. New Cathode Materials for Rechargeable Mg Batteries: Fast Mg Ion Transport and Reversible Copper Extrusion in $Cu_yMo_6S_8$ Compounds. *Chem. Commun.* **2007**, 4212–4214.
25. NuLi, Y. N.; Yang, J.; Li, Y. S.; Wang, J. L. Mesoporous Magnesium Manganese Silicate as Cathode Materials for Rechargeable Magnesium Batteries. *Chem. Commun.* **2010**, *46*, 3794–3796.
26. Tao, Z. L.; Xu, L. N.; Gou, X. L.; Chen, J.; Yuan, H. T. TiS_2 Nanotubes as The Cathode Materials of Mg-Ion Batteries. *Chem. Commun.* **2004**, 2080–2081.
27. Chiritescu, C.; Cahill, D. G.; Hguyen, N.; Johnson, D.; Bodapati, A.; Keblinski, P.; Zschack, P. Ultralow Thermal Conductivity in Disordered, Layered WSe_2 Crystals. *Science* **2007**, *315*, 351–353.
28. Boscher, N. D.; Carmalt, C. J.; Parkin, I. P. Atmospheric Pressure Chemical Vapor Deposition of WSe_2 Thin Films on Glass—Highly Hydrophobic Sticky Surfaces. *J. Mater. Chem.* **2006**, *16*, 122–127.
29. Fang, H.; Chuang, S.; Chang, T. C.; Takei, K.; Takahashi, T.; Javey, A. High-Performance Single Layered WSe_2 p-FETs with Chemically Doped Contacts. *Nano Lett.* **2012**, *12*, 3788–3792.
30. Feng, Z. Z.; NuLi, Y. N.; Wang, J. L.; Yang, J. Study of Key Factors Influencing Electrochemical Reversibility of Magnesium Deposition and Dissolution. *J. Electrochem. Soc.* **2006**, *153*, C689–C693.
31. Nam, K. T.; Kim, D. W.; Yoo, P. J.; Chiang, C. Y.; Meethong, N.; Hammond, P. T.; Chiang, Y. M.; Belcher, A. M. Virus-Enabled Synthesis and Assembly of Nanowires for Lithium Ion Battery Electrodes. *Science* **2006**, *312*, 885–888.
32. Liu, B.; Wang, X. F.; Liu, B. Y.; Wang, Q. F.; Tan, D. S.; Song, W. S.; Hou, X. J.; Chen, D.; Shen, G. Z. Advanced Rechargeable Lithium-Ion Batteries Based on Bendable $ZnCo_2O_4$-Urchins-on-Carbon-Fibers Electrodes. *Nano Res.* **2013**, *6*, 525–534.
33. Wang, Y. G.; Li, H. Q.; Xia, Y. Y. Ordered Whiskerlike Polyaniline Grown on The Surface of Mesoporous Carbon and Its Electrochemical Capacitance Performance. *Adv. Mater.* **2006**, *18*, 2619–2623.
34. Besenhard, J. O.; Winter, M. Advances in Battery Technology: Rechargeable Magnesium Batteries and Novel Negative-Electrode Materials for Lithium Ion Batteries. *ChemPhysChem* **2002**, *3*, 155–159.
35. Reshak, A. H.; Auluck, S. Electronic and Optical Properties of *2H*-WSe_2 Intercalated with Copper. *Phys. Rev. B* **2003**, *68*, 195107–195111.
36. Blochl, P. E. Projector Augmented-Wave Method. *Phys. Rev. B* **1994**, *50*, 17953–17979.
37. Porezag, D.; Pederson, M. R. Infrared Intensities and Raman-Scattering Activities within Density-Functional Theory. *Phys. Rev. B* **1996**, *54*, 7830–7836.